Ceramics-Silikáty 68 (4), 505-515 (2024)
www.ceramics-silikaty.cz doi: 10.13168/cs.2024.0049

ACHIEVING SUPERIOR ENERGY STORAGE PERFORMANCE IN BARIUM TITANATE CERAMICS VIA A RARE EARTH CO-DOPING STRATEGY

#MAHMOUD. S. ALKATHY*, H. A. KASSIM**, MANSOUR K. GATASHEH***, J PUNDAREEKAM GOUD****, JOSE A. EIRAS*

*Department of Physics, Federal University of São Carlos, São Carlos, SP 13565-905, Brazil
**Department of Physics, College of Science, P.O. BOX 2455, King Saud University, Riyadh 11451, Saudi Arabia
***Department of Biochemistry College of Science, King Saud University, P.O. Box 2455, Riyadh 11451, Saudi Arabia
****Department of Physics, Koneru Lakshmaiah Education Foundation, Bowrampet, Hyderabad, 500043, Telangana, India

#E-mail: alkathy@df.ufscar.br

Submitted June 26, 2024, accepted July 17, 2024

Keywords: Co-doping, Dielectric constant, Ferroelectric, Breakdown strength, Energy storage density

This study describes the fabrication of polycrystalline ceramics $Ba_{1-x}(La_{1/3}, Nd_{1/3})_xTiO_3$ by a solid-state reaction technique. The room temperature X-ray diffraction analysis using Rietveld refinement confirmed the formation of a polycrystalline compound with a tetragonal crystal structure consisting of a single phase. Doping $BaTiO_3$ with La^{3+} and Nd^{3+} ions enhanced the relative permittivity at room temperature. The co-doped samples possess a much higher dielectric constant in the wide frequency range, an essential characteristic for producing ceramic capacitors. The P–E hysteresis loop of the investigated samples was performed at room temperature. The results show that the remnant polarisation decreased from 9.05 to 1.95 $\mu C \cdot cm^{-2}$ while the breakdown strength increased from 50 $kV \cdot cm^{-1}$ to 167 $kV \cdot cm^{-1}$ when the co-dopants rose from 0 to 8 %. Accordingly, the energy storage density increased from 0.265 to 1.182 $J \cdot cm^{-3}$, and the efficiency also increased from 30 % to 77 %. The BLNT 8 % sample is also very stable throughout a wide temperature range, making it a promising option for future energy storage applications.

INTRODUCTION

In materials science, the strategic manipulation of a material's composition has become a pivotal approach for tailoring the physical properties of ceramics. Due to downsizing, the widespread use of Internet of Things (IoT) networks, and the prevalence of mobile devices, the demand for sophisticated electronic components has proliferated. Materials with a large dielectric constant (>1000) have garnered significant attention in recent years [1–4]. The need for smaller electronic devices has prompted the investigation of materials with high dielectric constants since they can potentially reduce the size of devices while maintaining a high energy storage capacity [5, 6]. The dielectric characteristics of many high-permittivity materials have been studied [7–10]. Barium titanate ($BaTiO_3$) is essential in fabricating multilayer ceramic capacitors because of its high dielectric constant. However, its characteristics are often limited to a specific temperature range around the phase transition temperature (Tc) [11]. Modifications to its dielectric-temperature properties are required to broaden the range of applications for $BaTiO_3$ in multi-electronic devices. This may be accomplished by introducing additional elements by doping the Ba^{2+}, Ti^{4+}, or both sites [12–16]. The electric and dielectric characteristics of $BaTiO_3$ are dependent on the crystallographic distortion, which is an intrinsic characteristic of its perovskite structure [17–19]. Significant progress has been made in the field of permittivity at ambient temperatures. For instance, researchers have discovered that the lattice structure is distorted by replacing foreign elements, such as Mg^{2+} [20], Cr^{3+}, $Fe^{3+,}$ and Ni^{2+} [21], at the Ti^{4+} site of the $BaTiO_3$ (BT) matrix, resulting in an improved temperature stability over a wide range. Furthermore, introducing co-doping in $BaTiO_3$ ceramics has significantly increased the dielectric permittivity while maintaining a low level of dielectric loss [22–26]. Furthermore, there is ongoing research about the impact of doping on the energy storage density and efficiency of BT. Several researchers have extensively studied the interaction between the microstructure, dielectric behaviour, and energy storage density and efficiency of BT-based ceramics, highlighting their significant importance [27-30].

In the pursuit of enhancing the performance of ceramic materials for electronic applications, this study focuses on the effect of La^{3+} and Nd^{3+} on the physical properties of $BaTiO_3$ ceramics. Incorporating La^{3+} and Nd^{3+} ions into the $BaTiO_3$ matrix significantly enhances the room-temperature relative permittivity. A critical aspect of the study is the examination of the dielectric properties at room temperature, showcasing

a remarkable increase in the dielectric constant for the co-doped samples. All these results show that La^{3+} and Nd^{3+} co-doped $BaTiO_3$ ceramics could be valuable materials for future electronics, especially those that store energy. The study contributes to understanding these ceramics' structural and dielectric properties and underscores their potential for advancing electronic technologies.

EXPERIMENTAL

The preparation of the $BaTiO_3$ samples with the La^{3+} and Nd^{3+} co-substitution was carried out using a traditional solid-state approach. The sample was prepared using the generic formula $Ba_{1-x}(La_{1/3},Nd_{1/3})_xTiO_3$, abbreviated as (BLNT*x*), where x = 0, 2 %, 4 %, and 8 %. $BaCO_3$, La_2O_3, Nd_2O_3, and TiO_2, all of which either have a purity of 99.99 % and 99.98 % were used as the initial substances to produce the $BaTiO_3$ powder with co-doped La^{3+} and Nd^{3+} ions. The mixture was pulverised and subjected to ball milling for 12 hours. A conventional furnace was used to calculate the milled powder. The desired temperature was maintained at 1100 °C for 8 hours, while the heating and cooling rate was set at 5 °C per minute. A pellet with a height of 1 mm and a diameter of 8 mm was formed by pressing the powder using a binder called polyvinyl alcohol (PVA) at a concentration of 1 %. The pressing process included applying a unidirectional pressure of 90 MPa. The pellets were subjected to a temperature of 500 °C for 1 hour to evaporate the binder. This was achieved using a muffle furnace with a heating and cooling rate of 2 °C per minute. Ultimately, the samples underwent sintering in the presence of air at a temperature of 1350 °C for 5 hours. This process was carried out using a conventional furnace with a heating and cooling rate of 5 °C per minute. The ceramics were phase-confirmed using an X-ray diffraction (XRD) analysis conducted with a Bruker D8 X-ray diffractometer with a Cu Kα wavelength of 1.5418 Å. The full-prof refinement program determined the lattice parameters and unit cell volume. A layer of silver paste was placed on both sides of the sample discs to examine the dielectric characteristics, creating a capacitor shape. The dielectric permittivity characteristics of the sintered samples were assessed using an Agilent E4292A impedance analyser, which operates from 60 Hz to 2 MHz. The *P–E* hysteresis loop was investigated at an ambient temperature of 10 Hz using a Radiant Precision Premier II Analyser.

RESULTS AND DISCUSSION

The X-ray diffraction patterns of the BLNTx ceramic powders are shown in Figure 1a. All the samples showed structural evidence of being perovskite. The XRD patterns, which are in good agreement with JCPDS (01-075-0583) [31], support the tetragonal P4mm space group. Therefore, the P4mm space group is used to index the XRD peaks. Thus, the complete diffusion of La^{3+} and Nd^{3+} ions is fully diffused throughout the BT lattice. On the right side of Figure 1a, the (002) and (200) splitting patterns are magnified so that the intensity of the (002) peaks is seen to increase and the (200) peak intensity decreases with the increased co-dopant ions. Also, it has been found that when the substitution rates rise, the peaks begin to blend. Peaks (002) and (200) combined to form a single broad peak in La^{3+} and Nd^{3+}. The peak splitting is more significant in the BT than in

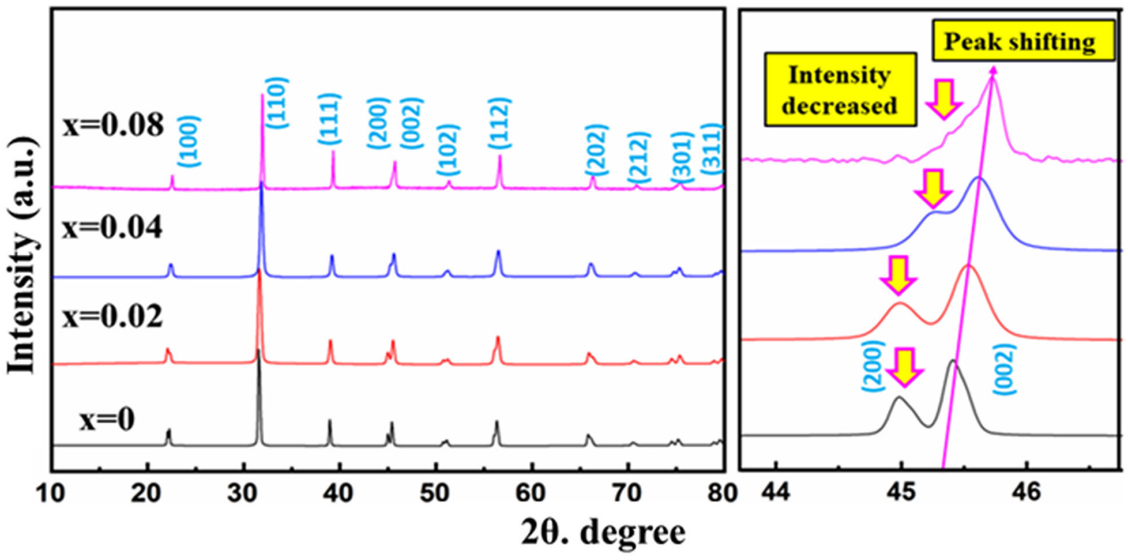

a)

Figure 1. XRD patterns of the BLNTx ceramics measured at room temperature, with the right graph showing the peak shifting and splitting by making the (200/002) diffraction pattern bigger (a). *(Continue on next page)*

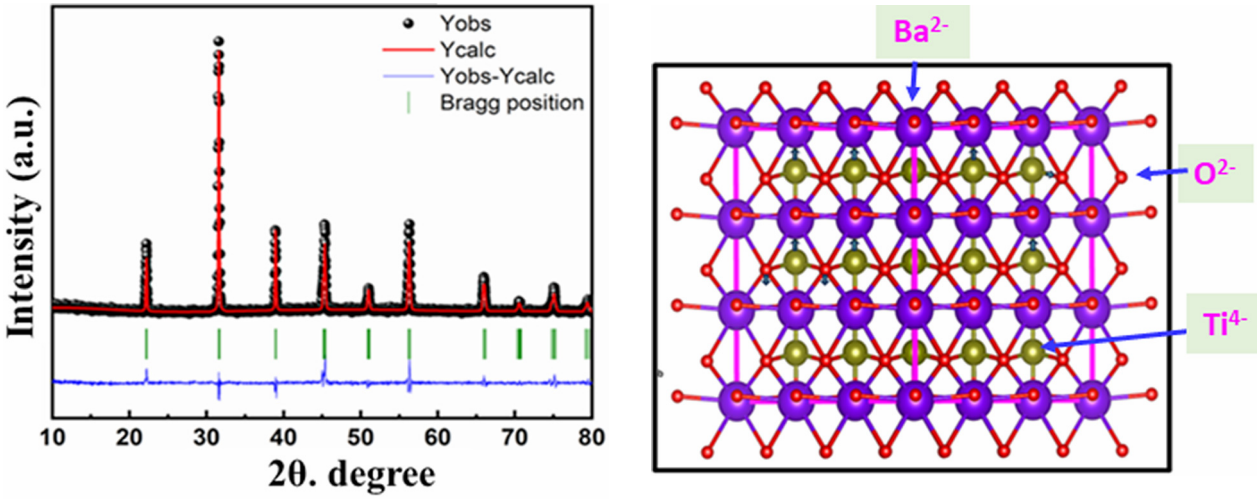

b) c)

Figure 1. XRD refinement analysis of BLNT 8 % (b); a schematic diagram of the BT supercell's tetragonal structure visualised by VESTA software (c).

the co-doped samples. In addition, it has been discovered that the XRD patterns shift to the high-angle side when the La^{3+} and Nd^{3+} concentrations increase. Substituting La^{3+} and Nd^{3+} for Ba^{2+} in the BT unit cell explains the observed lattice contraction. Using the full-prof software program, the Rietveld refinement approach was used with this XRD data to analyse these samples' lattice parameters and structural changes, as seen in Figure 1b. In the first step of the Rietveld procedure for pure BT, the locations of the atoms are fixed by the non-centrosymmetric P4mm space group with Ba^{2+}, La^{3+}, and Nd^{3+} at the origin (000). The linear interpolation technique is used to evaluate the background. We use a model based on the asymmetric pseudo-Voight function for the Bragg peaks [32]. Constraints that can be refined are those that can be adjusted, such as the size, lattice, location, and profile of an object. Iterative improvements brought close agreement between the theoretical predictions and the empirical observations. All the samples' refined *R*-factors (R_{wp}, R_{exp}) also fall within an acceptable range of <10 %. Table 1 displays the calculated a, c, V, and c/a lattice characteristics and volumes. Overall, it is found that when the La^{3+} and Nd^{3+} concentrations grow, the unit cell volume and lattice parameter decrease. The following factors account for the decline: the La^{3+} (XII, 1.36 Å) and Nd^{3+} (XII, 1.27 Å) ions could have lower ionic radii than the Ba^{2+} (XII, 1.61 Å) ions [33]. The reduced electrostatic repulsion between nearby ions causes the crystal lattice to shrink when smaller ions are substituted for bigger ones [34]. The actual behaviour may vary depending on the crystal structure, the ion sizes being replaced, and the solid solution system specifics. The resultant lattice parameters are sensitive to several variables, including the charge, ionic radius, and crystal field effects [35]. For example, in electronic devices, sensors, and piezoelectric devices,

Table 1. Structural parameters obtained from the XRD data refinement using the full-prof software for BLNTx ceramics measured at room temperature.

Sample	BLNT0	BLNT0.02	BLNT0.04	BLNT0.08
Crystal system	Tetragonal	Tetragonal	Tetragonal	Tetragonal
a = b (Å)	3.9992	3.9989	3.9972	3.9960
c (Å)	4.0198	4.0176	4.0147	4.0124
V (Å)3	64.2910	64.2458	64.1440	64.0702
α = β = γ (o)	90	90	90	90
Tetragonality (c/a)	1.0052	1.0047	1.0044	1.0041
Space group	P4mm	P4mm	P4mm	P4mm
Space group no	99	99	99	99
D_p (nm)	74	67	62	57
R_p (%)	5.17	5.25	6.27	6.88
R_{wp} (%)	8.23	8.93	9.71	9.84
R_{ex} (%)	7.80	7.73	7.28	7.31
χ^2	1.11	1.33	1.77	1.99

the lattice parameters can affect the material's electrical, mechanical, and thermal properties by controlling the concentrations of the dopants [36]

The plot depicted in Figure 2a,b illustrates the association between the frequency and the dielectric permittivity (ε) as well as the loss tangent ($tan\ \delta$) of the BLNTx ceramics at room temperature. The measurements were conducted over a frequency range from 60 Hz to 2 MHz. Notably, the dielectric permittivity exhibits a positive correlation with lower frequencies and a negative correlation with higher frequencies. This behaviour is consistent with the typical response of dielectric materials. At lower frequencies, there is a pronounced alignment of dipoles with the applied field, leading to a higher dielectric permittivity. This is due to the material's ability to polarise in response to an applied electric field, expressed as the dielectric constant or relative permittivity (symbol ε). At higher frequencies, the inability of dipoles to align themselves with the electric field results in reduced interfacial polarisation and a lower dielectric constant [37-41]. At low frequencies, dipole alignments can respond fast enough to align with the electric field, leading to a higher dielectric constant. However, dipoles do not have sufficient time to align at very high frequencies, resulting in a lower dielectric constant. The dielectric constant remains relatively constant at these lower frequencies, reflecting its value in a static field. However, as the frequency increases, dipoles experience a delayed response to the electric field, resulting in a minor reduction in the dielectric constant. At higher frequencies, dipoles struggle to track the rapidly changing field, leading to a relatively constant dielectric permittivity, a phenomenon well-documented in the literature [42]. The Maxwell-Wagner model is considered to elucidate the frequency-dependent changes in dielectric permittivity. This model incorporates interfacial or space charge polarisation with Koop's phenomenological theory [43-44]. According to this model, dielectric materials consist of highly conductive grains separated by narrow borders from less conductive ones. When an external electric field is applied, charge carriers migrate from the grains and accumulate at the borders, resulting in significant polarisation and a high dielectric permittivity (ε). The decrease in the dielectric permittivity with the increasing frequency is attributed to the inertia of polarisation, causing a delayed response to the applied external electric field. This abnormal reaction leads to a reduction in the dielectric constant. In the lower frequency range, various forms of polarisation, including ionic, electronic, dipolar, and space charge polarisation, contribute significantly to the dielectric value, as observed in previous studies [44-45]. As the frequency increases, the impact of different polarisations diminishes, and at higher frequencies, only electronic and dipolar polarisations contribute to the overall polarisation. Consequently, a decrease in the dielectric permittivity is induced [44-47].

The dielectric constant and dielectric loss of BLNTx ceramics were measured at 1 kHz and within the 25-200 °C temperature range, as seen in Figure 2c.

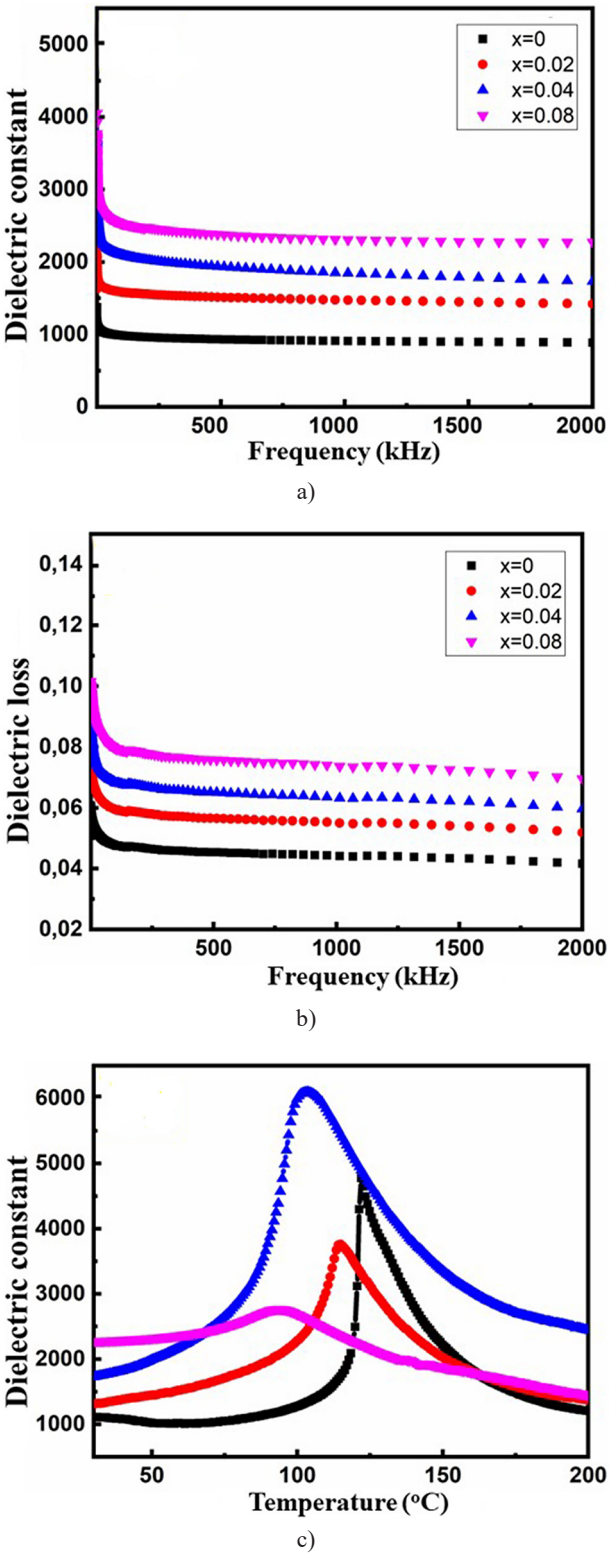

Figure 2. The relationship between the frequency (a) and the dielectric constant (b) and the loss tangent of sintered BLNTx ceramics, as determined at a frequency range of 60 to 2 MHz at room temperature.

The figure demonstrates that the dielectric constant for $x = 0$, $x = 2$ %, and $x = 4$ % exhibited a progressive rise and peaked at a specific Curie temperature, after which it declined. This denotes the change in state from ferroelectric to paraelectric, as seen in the transition phase [48–49]. However, in the case of the sample containing La^{3+} and Nd^{3+} ions co-doped in $BaTiO_3$ ceramics with a concentration of $x = 8$ %, the dielectric constant reached its maximum value. It stayed consistently high throughout a more comprehensive temperature range. Additionally, there was a minor rise in the dielectric constant at $T_c \sim 90$ °C. This observation suggests that the sample exhibits diffused phase transition behaviour. This behaviour may be attributed to several factors. As a result of changes in the microscopic composition, micropolar zones are combining to form micropolar areas. The order parameter is also linked to the local disorder mode owing to local strain [50]. Vugmeister [51] showed that the primary cause of diffuse phase transition (DPT) behaviour in mixed oxide compounds is the stochastic arrangement of the electrical strain field. When added to a perovskite structure, Aliovalent cations may alter the electrical properties by donating or accepting electrons. Furthermore, Figure 2c illustrates that the Curie temperature changed towards lower temperatures as the dopant concentrations increased. The variation in the Curie temperature (T_c) of $BaTiO_3$ ceramics resulting from the co-doping of La^{3+} and Nd^{3+} may be attributed to many factors. The search results did not specifically discuss the variables that affect the change in the Curie temperature in $BaTiO_3$ ceramics when rare-earth ions are added. Nevertheless, previous studies and specialised knowledge in this field suggest that the following factors might influence this phenomenon: (i) Interactions amongst the dopant ions: The presence of La^{3+} and Nd^{3+} ions may lead to interactions with the BTO host lattice, which might influence the crystal structure and ferroelectric characteristics of the material, thereby affecting the Curie temperature [52]. Adding La^{3+} ions to $BaTiO_3$ may modify its crystal structure, affecting the Curie temperature of the material [53]. The presence of La^{3+} and Nd^{3+} ions might modify the dielectric properties of the material, resulting in a variation in the Curie temperature [54]. The doping concentration of La^{3+} and Nd^{3+} may affect the change in the Curie temperature. Higher doping concentrations lead to a more significant decrease in the Curie temperature [55, 56]. The search results comprehensively comprehend the Curie temperature's behaviour in doped ceramics. However, they did not possess detailed knowledge of the exact parameters that cause the change when La^{3+} is added to $BaTiO_3$. Therefore, the criteria are drawn from the existing understanding of how dopant ions affect the properties of ferroelectric materials. Additional research and scientific inquiry are necessary to fully comprehend the process behind the change in Curie temperature when La^{3+} and Nd^{3+} are added to $BaTiO_3$ ceramics.

A ferroelectric hysteresis loop is a visual depiction of the ferroelectric properties of a substance, often defined by its polarisation reaction to an externally applied electric field. The observed hysteresis loop demonstrates how adding La^{3+} and Nd^{3+} dopant ions in $BaTiO_3$ ceramics affects the ferroelectric properties. This text details the essential parts of the ferroelectric hysteresis loop that can be seen in $BaTiO_3$ ceramics mixed with La^{3+} and Nd^{3+}. The hysteresis loop in Figure 3 shows the connection between the electric field (E) and the polarisation (P) of $BaTiO_3$ ceramics that have La^{3+} and Nd^{3+} added to them. This figure demonstrates how the polarisation varies based on the direction and strength of the electric field. Under conditions of large electric fields, the polarisation becomes saturated, reaching its maximum value. The saturation point is the highest level of polarisation that the material can achieve under specific circumstances. The polarisation (P_r) reduced from 9.05 to 1.95 $\mu C \cdot cm^{-2}$, but the breakdown strength increased from 50 $kV \cdot cm^{-1}$ to 170 $kV \cdot cm^{-1}$ as the co-dopants rose from 0 to 8 %. The loop offers valuable insights into the ferroelectric phase transition of doped $BaTiO_3$ ceramics. In large concentrations of co-dopant, the hysteresis loop narrows, providing confirmation of the diffused behaviour and suggesting the influence of doping on the material's properties. Co-doped $BaTiO_3$ ceramics, which possess regulated ferroelectric characteristics, are used in various devices, such as ferroelectric capacitors. A hysteresis loop is essential for evaluating materials for these specific applications. As the concentration of co-dopants increases in the present research, there is a proportional suppression of grain formation, leading to a decrease in the grain size [57-59]. Consequently, the number of grain boundaries and energy barriers increases. The grain boundary region demonstrates a reduced permittivity and a lower degree of ferroelectricity. Due to this, as the concentration of co-substituted elements increases, the remaining polarisation decreases. A decrease in the grain sizes explains this, as the report studied $BaTiO_3$ ceramics modified with La-doped A sites [60–62].

The effect of the grain size on the residual polarisation is a complex phenomenon attributed to several mechanisms, depending on the specific material and its properties. For example, in domain wall pinning, smaller grain sizes lead to a higher density of grain boundaries within the material [63]. These grain boundaries can act as obstacles to the movement of domain walls, regions within the material where the polarisation direction changes. When an external electric field is applied, these domain walls move, contributing to the overall polarisation of the material [64]. However, when the field is removed, the domain walls can become pinned at the grain boundaries, leading to lower residual polarisation in materials with smaller grain sizes [65]. Furthermore, charges can accumulate at the interface between different grains due to differences in the crystal structure, composition, or defects [66]. These charges at

the interface can help create a local electric field that is the opposite of the applied field. This can cause lower net polarisation and, as a result, lower residual polarisation in materials with smaller grains [66, 67]. The grain size of ceramics plays a crucial role in their energy storage performance, particularly for applications like capacitors and batteries.

To investigate the effect of La and Nd in the energy storage performance of $BaTiO_3$ ceramics we can theoretically estimate the energy storage parameters such as recoverable energy storage density, and energy storage efficiency using the following equations [68]:

$$W_{tot} = \int_P^{P_m} EdP \quad (1)$$

$$W_{rec} = \int_0^{P_m} EdP \quad (2)$$

$$\eta\,(\%) = \frac{\int_0^{P_m} EdP}{\int_P^{P_m} EdP} \quad (3)$$

Regarding the abovementioned equations, E denotes the external electric field, while P_m and P_r denote the maximum and remnant polarisations. We can see from these formulas that to achieve excellent performance in terms of energy storage, we need to generate a significant difference between the maximum polarisation (P_m) and the remnant polarisation (P_r). This can be accomplished by inducing a high P_m, low P_r, and high breakdown strength. From the ferroelectric results correlated with the microstructure, we can see that the sample with high co-doping content has a small rain size compared to others, resulting in an apparent change in the behaviour of the hysteresis loop (Figure 3d) and increasing the breakdown strength from 50 kV·cm^{-1} in the pure BT sample to 167 kV·cm^{-1} in the 8 % co-doping sample. Several variables affect the ceramic breakdown strength, but one of them is the effect of grain boundaries on the electrical characteristics, which helps to explain the correlation between grain size and breakdown voltage. The breakdown voltage of a ceramic material is the

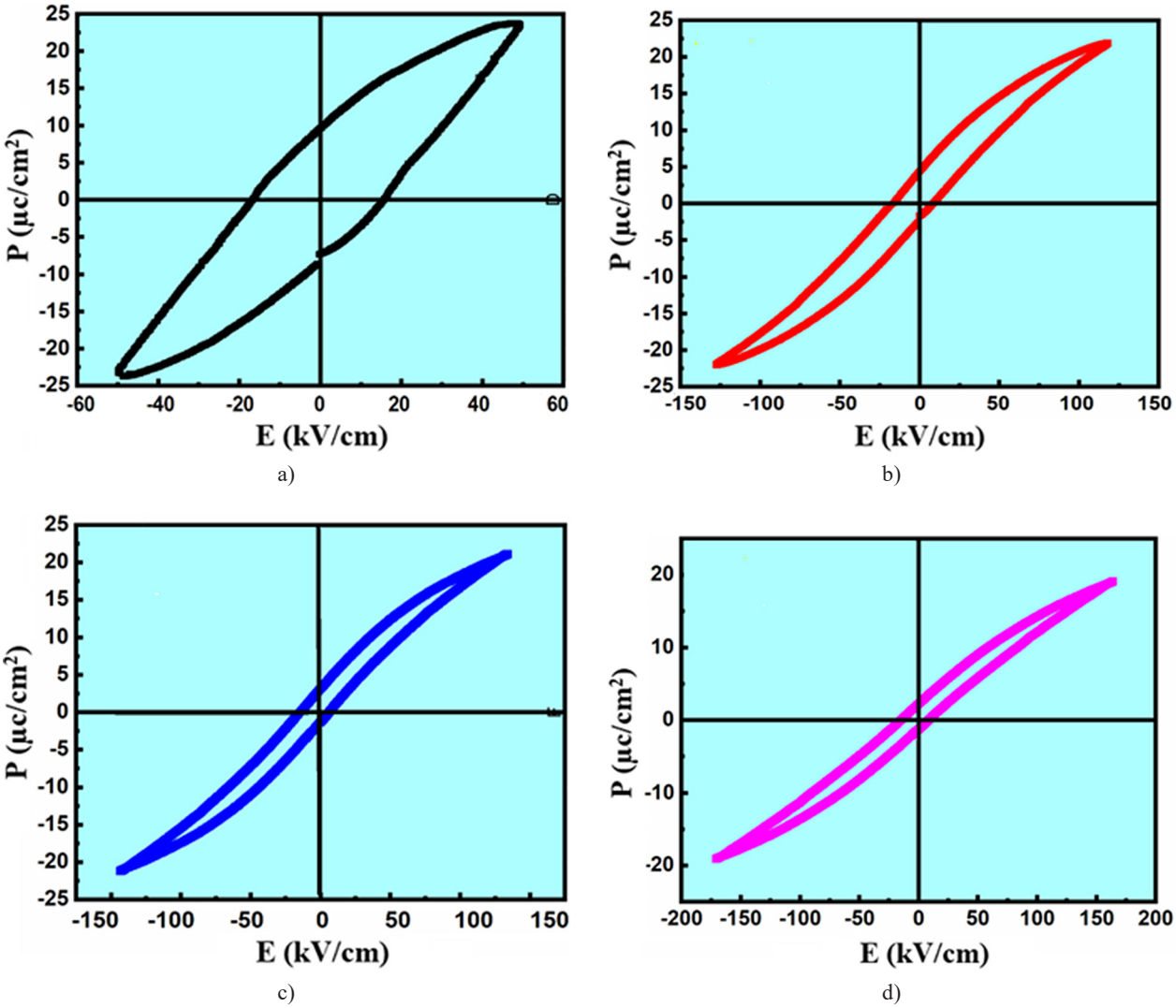

Figure 3. The hysteresis loops of the BLNTx ceramic at room temperature. The loops correspond to different La^{3+} and Nd^{3+} concentrations namely: a) x = 0, b) x = 2 %, c) x = 4 %, d) x = 8 %. The measurements were taken at a frequency of 10 Hz.

voltage at which its insulating qualities are no longer maintained, and its electrical conductivity becomes substantially higher [69]. The following are some ways a smaller grain size could raise the breakdown voltage: (i) Desensitisation of the grain boundary: The grain boundaries serve as connections between the individual grains in a ceramic substance. The density of grain boundaries is directly proportional to the grain size [70]. With fewer grain boundaries, charge carriers (ions or electrons) have fewer places to move. A greater breakdown voltage and increased resistance can emerge from a decrease in the number of possible electrical conduction paths. A more homogenous microstructure is often the result of small grain sizes, which enhance homogeneity [71]. Electrical characteristics are more uniformly distributed in ceramics that have a stable grain size. A lower chance of early failure due to localised defects or abnormalities and a more predictable reaction to applied electric fields are both outcomes of this uniformity. (ii) Abnormalities in large grains, such as voids or inclusions, may cause localized stress concentrations [72]. Lessening the impact of these imperfections, smaller grains help to disperse stress more uniformly throughout the material. Distributing the load uniformly may increase the breakdown voltage and decrease the chances of localised failure. Based on the above equations and discussions, the energy storage density increased with the co-dopant concentrations, which plays a significant role in developing energy storage devices for the next-generation applications.

The unipolar P–E hysteresis loops in Figure 4 are used to evaluate the energy storage performance of materials. These loops provide insights into the relationship between the polarisation and the electric field, allowing for the estimation of stored energy and hysteresis losses [73-76]. The area enclosed by the hysteresis loop

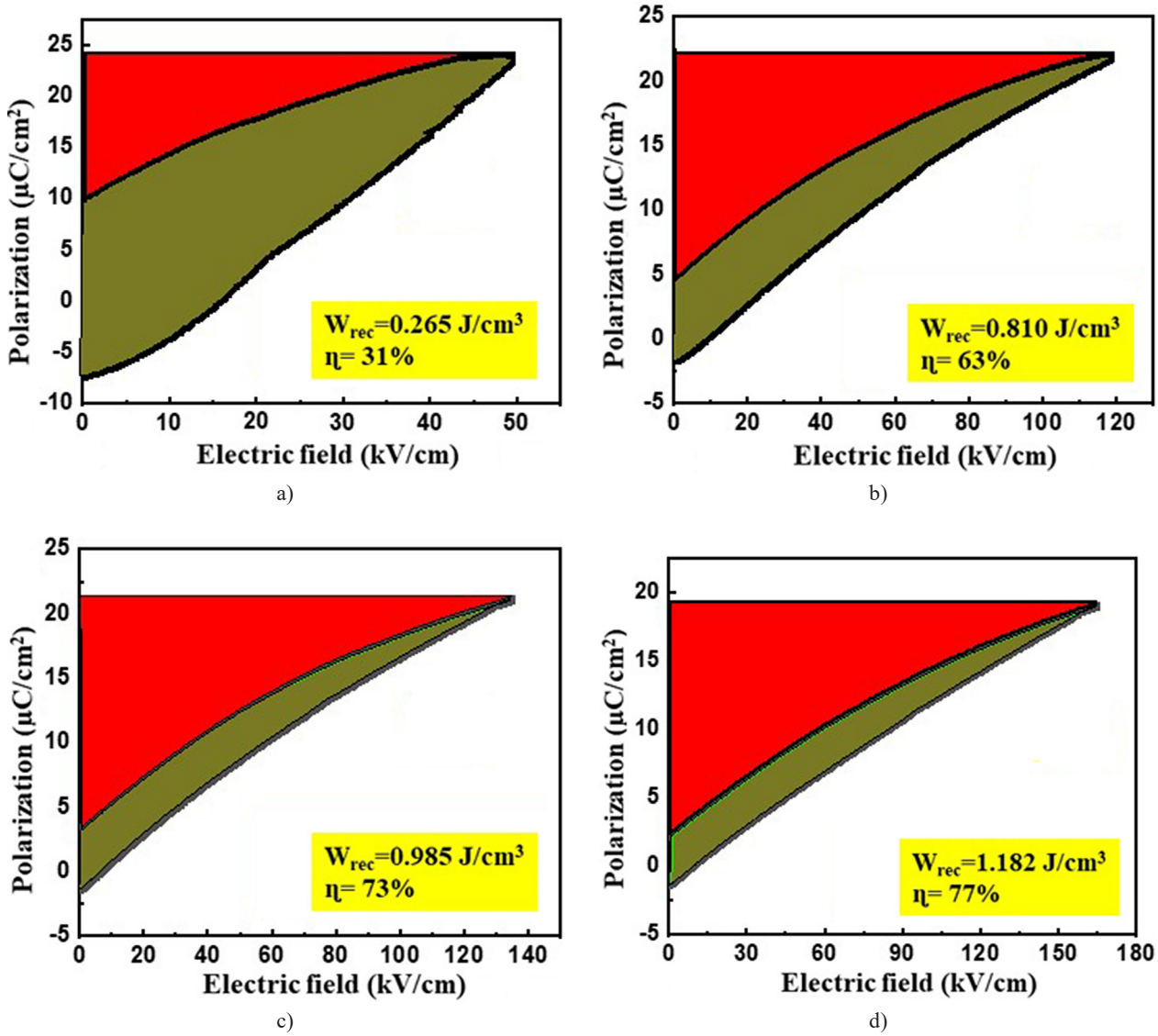

Figure 4. The unipolar P–E hysteresis loops obtained from measurements conducted at 10 Hz for the $BaTiO_3$ ceramics co-doped with La and Nd. The figure includes four subplots, each corresponding to a different doping level: a) $x = 0$, b) $x = 2$ %, c) $x = 4$ %, and d) $x = 8$ %.

represents the energy stored, while the hysteresis loss indicates the energy not recovered completely. The material's grain size plays a crucial role in its energy storage performance, with smaller grain sizes leading to lower residual polarisation and high energy storage efficiency, as shown in Figure 4d.

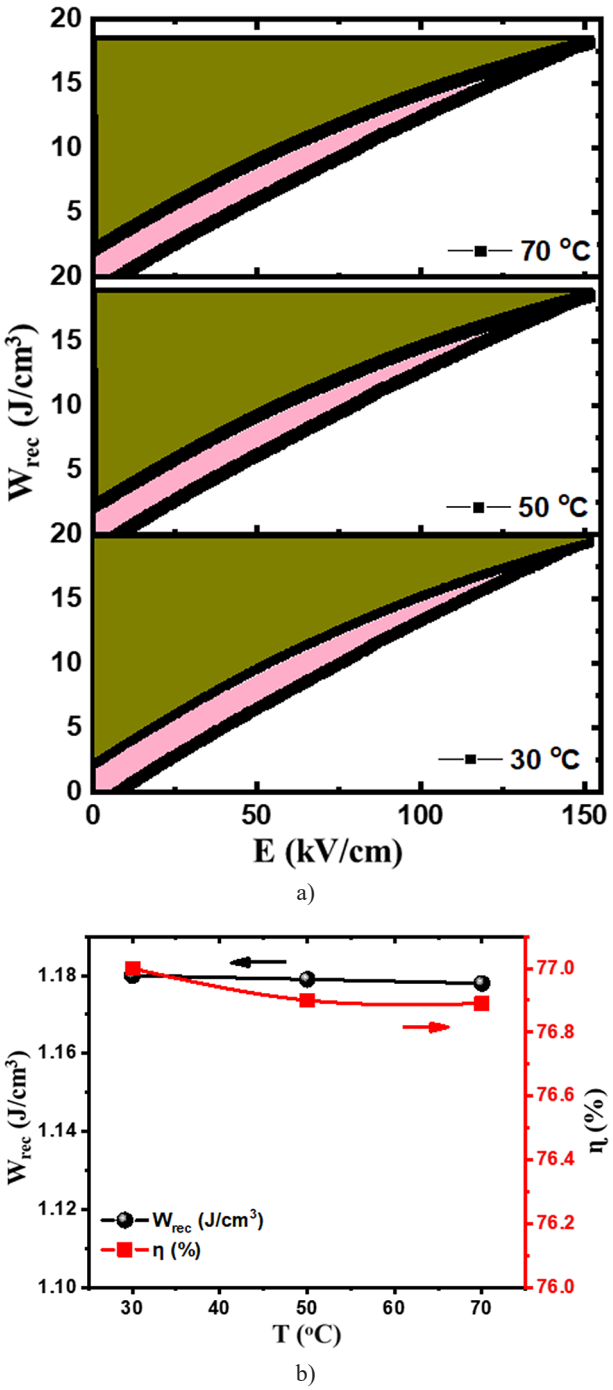

Figure 5. The unipolar P–E hysteresis loops obtained from measurements conducted at 10 Hz for BLNT 8 % ceramics measured at three different temperatures to investigate the stability of the energy storage performance (a); the variation in the energy storage density and energy storage efficiency with the temperature (b).

Finally, we discuss the stability of our optimised BNLT 8 % sample at different temperatures. Temperature stability is widely recognised as one of the most important characteristics of energy storage technologies. Figure 5a shows the measurement of the unipolar P–E loops at f = 10 Hz and E = 155 kV·cm^{-1} as a function of T, ranging from 30 °C to 70 °C. As can be observed, the P_{max} is nearly constant across the temperature range under consideration. Figure 5b displays the necessary W_{rec} and η data. The results show that Wrec and η are modestly lowered, indicating stability at measured temperatures. The findings indicate that the BNLT8% could be useful for energy storage applications.

CONCLUSION

This study utilised a solid-state reaction technique to produce $Ba_{1-x}(La_{1/3}, Nd_{1/3})_xTiO_3$ ceramics with a tetragonal crystal structure. The co-doping of La^{3+} and Nd^{3+} ions enhanced the permittivity and altered the ferroelectric behaviour. The co-doped samples exhibited a high dielectric constant and showed a promising performance as a ceramic capacitor. The investigation into the P–E hysteresis loops revealed a decrease in the remnant polarisation and a substantial increase in the breakdown strength with the increasing co-dopant concentration. These electrical property modifications directly influenced the energy storage, showcasing a significant enhancement in the density from 0.265 to 1.182 J·cm^{-3} and the efficiency from 30 % to 77 % as the co-dopants increased from 0 to 8 %. These findings highlight the potential of La^{3+} and Nd^{3+} co-doped $BaTiO_3$ ceramics for future electronic devices, particularly in energy storage applications, due to the improved dielectric properties and enhanced energy storage performance.

Acknowledgments

The authors sincerely thank the financial support of the Sao Paulo Research Foundation (FAPESP: Grant No. 2017/13769-1) and FAPESP: Grant No. (2023/05716-6). Dr. Mansor sincerely thanks the researchers for supporting project number (RSP2024R393) at King Saud University in Riyadh, Saudi Arabia.

REFERENCES

1. Wang Y., Jie W., Yang C., Wei X., Hao J. (2019): Colossal permittivity materials as superior dielectrics for diverse applications. *Advanced Functional Materials, 29*(27), 1808118. doi: 10.1002/adfm.201808118
2. Liang L., Shi Z., Tan X., Sun S., Chen M., et al. (2022): largely improved breakdown strength and discharge efficiency of layer-structured nanocomposites by filling with a small loading fraction of 2D zirconium phosphate nanosheets. *Advanced Materials Interfaces*, *9*(3), 2101646. doi: 10.1002/admi.202101646

3. Alkathy M. S., Raju, K. J. (2018): Structural, dielectric, electromechanical, piezoelectric, elastic and ferroelectric properties of lanthanum and sodium co-substituted barium titanate ceramics. *Journal of Alloys and Compounds*, *737*, 464-476. doi: 10.1016/j.jallcom.2017.12.121
4. ,M. S., Pattipaka S., Gatasheh M. K., Zabotto F. L., Eiras J. A. (2024): Manganese and magnesium co-doped barium titanate: A route towards enhanced energy storage performance via defect dipoles engineering. *Journal of Inorganic and Organometallic Polymers and Materials*, *34*(3), 1193-1207. doi: 10.1007/s10904-023-02891-7
5. Zhou Y., Qi H., Yang J., Bo Z., Huang F., et al. (2021): Two-birds-one-stone: multifunctional supercapacitors beyond traditional energy storage. *Energy & Environmental Science*, *14*(4), 1854-1896. doi: 10.1039/D0EE03167D
6. Zu L., Zhang W., Qu L., Liu L., Li W., Yu A., Zhao D. (2020): Mesoporous materials for electrochemical energy storage and conversion. *Advanced Energy Materials*, *10*(38), 2002152. doi: 10.1002/aenm.202002152
7. Dang Z. M., Yuan J. K., Yao S. H., Liao R. J. (2013): Flexible nanodielectric materials with high permittivity for power energy storage. *Advanced Materials*, *25*(44), 6334-6365. doi: 10.1002/adma.201301752
8. Wang Y., Jie W., Yang C., Wei X., Hao J. (2019): Colossal permittivity materials as superior dielectrics for diverse applications. *Advanced Functional Materials*, *29*(27), 1808118. doi: 10.1002/adfm.201808118
9. Zhou W., Cao G., Yuan M., Zhong S., Wang Y., et al. (2023): Core–shell engineering of conductive fillers toward enhanced dielectric properties: a universal polarization mechanism in polymer conductor composites. *Advanced Materials*, *35*(2), 2207829. doi: 10.1002/adma.202207829
10. Alkathy M. S., Raju K. J., Eiras, J. A. (2021): Colossal dielectric permittivity and high energy storage efficiency in barium strontium titanate ceramics co-doped with bismuth and lithium. *Journal of Physics D: Applied Physics*, *54*(12), 125501. doi: 10.1088/1361-6463/abd12b
11. Zhao C., Huang Y., Wu J. (2020): Multifunctional barium titanate ceramics via chemical modification tuning phase structure. *InfoMat*, *2*(6), 1163-1190. doi: 10.1002/inf2.12147
12. Patil R. P., Karanjekar A. N., Gaikwad V. B., Jain G. H., Shinde S. D. (2022): Doping-induced diffused phase transition triggers gas-sensing performance of Sn-doped $BaTiO_3$ nanostructures. *Surface and Interface Analysis*, *54*(1), 25-36. doi: 10.1002/sia.7012
13. Huang Y., Zhao C., Zhong S., Wu J. (2021): Highly tunable multifunctional $BaTiO_3$-based ferroelectrics via site selective doping strategy. *Acta Materialia*, *209*, 116792. doi: 10.1016/j.actamat.2021.116792
14. Cai E., Gu H., Liu Q. (2023): Electrical property optimization of $BaTiO_3$-based lead-free piezoceramics by chemical doping. *Journal of the American Ceramic Society*, *106*(11), 6717-6731. doi:10.1111/jace.19293
15. Arshad M., Du H., Javed M. S., Maqsood A., Ashraf I., et al. (2020): Fabrication, structure, and frequency-dependent electrical and dielectric properties of Sr-doped $BaTiO_3$ ceramics. *Ceramics International*, *46*(2), 2238-2246. doi: 10.1016/j.ceramint.2019.09.208
16. Alkathy M. S., JamesRaju K. C. (2017): Study of diffuse PhaseTransition behavior in Bi and Li Co-substituted barium titanate ceramics. *Journal of Electroceramics*, *38*, 63-73. doi: 10.1007/s10832-016-0060-z
17. Beuerlein M. A., Kumar N., Usher T. M., Brown-Shaklee H. J., Raengthon N., et al. (2016): Current understanding of structure–processing–property relationships in $BaTiO_3$–$Bi(M)O_3$ dielectrics. *Journal of the American Ceramic Society*, *99*(9), 2849-2870. doi: 10.1111/jace.14472
18. Ihlefeld J. F., Harris D. T., Keech R., Jones J. L., Maria J. P., Trolier-McKinstry S. (2016): Scaling effects in perovskite ferroelectrics: fundamental limits and process-structure-property relations. *Journal of the American Ceramic Society*, *99*(8), 2537-2557. doi: 10.1111/jace.14387
19. Ghosh D., Sakata A., Carter J., Thomas P. A., Han H., Nino J. C., Jones J. L. (2014): Domain wall displacement is the origin of superior permittivity and piezoelectricity in $BaTiO_3$ at intermediate grain sizes. *Advanced Functional Materials*, *24*(7), 885-896. doi: 10.1002/adfm.201301913
20. Cai W., Fu C. L., Gao J. C., Zhao C. X. (2011): Dielectric properties and microstructure of Mg doped barium titanate ceramics. *Advances in Applied Ceramics*, *110*(3), 181-185.
21. Choudhary R., Singh V., Singh A., Sachdev S., Kumar P. (2023): A comparative study on the effect of Cr^{3+}, Fe^{3+} and Ni^{2+} substitution on the dielectric, ferroelectric and electrocaloric response of BST ceramics. *Ceramics International*, *49*(22), 35145-35156. doi: 10.1016/j.ceramint.2023.08.187
22. Meng Y., Liu K., Zhang X., Lei X., Chen J., et al. (2022): Defect engineering in rare-earth-doped $BaTiO_3$ ceramics: Route to high-temperature stabilit y of colossal permittivity. *Journal of the American Ceramic Society*, *105*(9), 5725-5737. doi: 10.1111/jace.18512
23. Luo G., Zhang G., Zhang Y., Li A., Sun Y., Tu R., Shen Q. (2023): Wide temperature range of stable dielectric properties in relaxor $BaTiO_3$-based ceramics by co-doping synergistic engineering. *Materials Chemistry and Physics*, *302*, 127629. doi: 10.1016/j.matchemphys.2023.127629
24. Wang Z., Chen H., Nian W., Fan J., Li Y., Wang X. (2019): Bismuth oxide modified europium and niobium co-doped titanium dioxide ceramics: colossal permittivity and low dielectric loss design. *Journal of Alloys and Compounds*, *777*, 317-324. doi: 10.1016/j.jallcom.2018.10.366
25. Alkathy M. S., Rahaman A., Mastelaro V. R., Zabotto F. L., Milton F. P., Eiras J. A. (2023): Achieving high energy storage density simultaneously with large efficiency and excellent thermal stability by defect dipole, and microstructural engineering in modified-$BaTiO_3$ ceramics. *Journal of Alloys and Compounds*, *934*, 167887. doi: 10.1016/j.jallcom.2022.167887
26. Alkathy M. S., Rahaman A., Mastelaro V. R., Milton F. P., Zabotto F. L., et al. (2023): Enhanced energy-storage density of $BaTi_{0.95}Zr_{0.05}O_3$ via generation of defect dipoles upon lithium-doping. *Materials Chemistry and Physics*, *294*, 127032. doi: 10.1016/j.matchemphys.2022.127032
27. Hu Y. C., Dang S. T., Cao J. Q., Zhang W. L., Zai Y. J., Xu P. S., Wang X. W. (2023): $Bi(Li_{1/2}Nb_{1/2})O_3$ addition inducing improved energy storage performance in lead-free BCZT ceramics. *Applied Physics A*, *129*(8), 602. doi: 10.1007/s00339-023-06879-5
28. Chen S. Y., Liu R., Zheng Y. P., Shi Y. J., Dang S. T., et al. (2023): Enhanced energy storage properties of $Ba_{0.85}Ca_{0.15}Zr_{0.1}Ti_{0.9}O_3$ ceramics doped with $BiFeO_3$. *Journal of Alloys and Compounds*, *936*, 168015. doi: 10.1016/j.jallcom.2022.168015
29. Dang S. T., Xue L. L., He L. F., Shi Y. C., Li H. N., et al. (2022): Dielectric and energy storage properties of

$Ba_{0.85}Ca_{0.15}Zr_{0.1}Ti_{0.9}O_3$ ceramics with different aging temperature during the sol-gel process. *Journal of Materials Science: Materials in Electronics*, *33*(35), 26100-26112. doi: 10.1007/s10854-022-09297-0

30. Wang X. W., Shi X. N., Zhang R. Y., Shi Y. C., Liang Y. F., et al. (2022): Effect of Co doping on microstructure, dielectric, and energy storage properties of BCZT ceramics. *Journal of Materials Science: Materials in Electronics*, *33*(25), 20399-20412. doi: 10.1007/s10854-022-08856-9
31. Deng Z., Dai Y., Chen W., Pei X., Liao J. (2010): Synthesis and characterization of bowl-like single-crystalline $BaTiO_3$ nanoparticles. *Nanoscale Research Letters*, *5*, 1217-1221. doi: 10.1007/s11671-010-9629-7
32. Dinnebier R., Scardi P. (2021): X-ray powder diffraction in education. Part I. Bragg peak profiles. *Applied Crystallography*, *54*(6), 1811-1831. doi: 10.1107/S1600576721009183
33. Shannon R. D. (1976): Revised effective ionic radii and systematic studies of interatomic distances in halides and chalcogenides. *Foundations of Crystallography*, *32*(5), 751-767. doi: 10.1107/S0567739476001551
34. Walsh A. (2015): Principles of chemical bonding and band gap engineering in hybrid organic–inorganic halide perovskites. *The Journal of Physical Chemistry C*, *119*(11), 5755-5760. doi: 10.1021/jp512420b
35. Mullens B. G., Zhang Z., Avdeev M., Brand H. E., Cowie B. C., et al. (2021): Effect of Long-and Short-Range Disorder on the Oxygen Ionic Conductivity of $Tm_2(Ti_{2-x}Tm_x)O_{7-x/2}$ "Stuffed" Pyrochlores. *Inorganic Chemistry*, *60*(7), 4517-4530. doi: 10.1021/acs.inorgchem.0c03363
36. Tian Y., Cao L., Qin P., Sun S., Gong Y., et al. (2019): Piezoelectric and thermophysical performances of La^{3+} and Ir^{4+} co-doped $Ba_{0.95}Ca_{0.05}Ti_{0.94}Zr_{0.06}O_3$ ceramics. *Ceramics International*, *45*(10), 12825-12831. doi: 10.1016/j.ceramint.2019.03.203
37. Quan B., Liang X., Ji G., Cheng Y., Liu, W., et al. (2017): Dielectric polarization in electromagnetic wave absorption: review and perspective. *Journal of Alloys and Compounds*, *728*, 1065-1075. doi: 10.1016/j.jallcom.2017.09.082
38. Ahmad Z. (2012). Polymer dielectric materials. In *Dielectric material*. IntechOpen. doi: 10.5772/50638
39. Gao R., Zhang Q., Xu Z., Wang Z., Chen G., et al. (2019): A comparative study on the structural, dielectric and multiferroic properties of $Co_{0.6}Cu_{0.3}Zn_{0.1}Fe_2O_4$ / / $Ba_{0.9}Sr_{0.1}Zr_{0.1}Ti_{0.9}O_3$ composite ceramics. *Composites Part B: Engineering*, *166*, 204-212. doi: 10.1016/j.compositesb.2018.12.010
40. Wu H., Xu R., Zhou C., Xing S., Zeng Z., et al. (2022): Effect of core size on the magnetoelectric properties of $Cu_{0.8}Co_{0.2}Fe_2O_4$ / $Ba_{0.8}Sr_{0.2}TiO_3$ ceramics. *Journal of Physics and Chemistry of Solids*, *160*, 110314. doi: 10.1016/j.jpcs.2021.110314
41. Gao R., Qin X., Zhang Q., Xu Z., Wang Z., et al. (2019): Enhancement of magnetoelectric properties of (1 – x) $Mn_{0.5}Zn_{0.5}Fe_2O_{4-x}Ba_{0.85}Sr_{0.15}Ti_{0.9}Hf_{0.1}O_3$ composite ceramics. *Journal of Alloys and Compounds*, *795*, 501-512. doi: 10.1016/j.jallcom.2019.05.013
42. Chandrasekhar M., Kumar P. (2016): Microwave sintered sol-gel derived $BaTiO_3$ and $Ba_{0.95}La_{0.05}TiO_3$ ceramic samples for capacitor applications. *Ceramics International*, *42*(9), 10587-10592. doi: 10.1016/j.ceramint.2016.03.135
43. Koops C. G. (1951): On the dispersion of resistivity and dielectric constant of some semiconductors at audiofrequencies. *Physical review*, *83*(1), 121. doi: 10.1103/PhysRev.83.121
44. Mishra P., Kumar P. (2012): Effect of sintering temperature on dielectric, piezoelectric and ferroelectric properties of BZT–BCT 50/50 ceramics. *Journal of Alloys and Compounds*, *545*, 210-215. doi: 10.1016/j.jallcom.2012.08.017
45. Singh A. K., Goel T. C., Mendiratta R. G., Thakur O. P., Prakash C. (2002): Dielectric properties of Mn-substituted Ni–Zn ferrites. *Journal of Applied Physics*, *91*(10), 6626-6629.
46. Zhu Y. F., Zhang Z., Litt, M. H., Zhu L. (2018): High dielectric constant sulfonyl-containing dipolar glass polymers with enhanced orientational polarization. *Macromolecules*, *51*(16), 6257-6266. doi: 10.1021/acs.macromol.8b00923
47. Qiu J., Gu Q., Sha Y., Huang Y., Zhang M., Luo Z. (2022): Preparation and application of dielectric polymers with high permittivity and low energy loss: A mini review. *Journal of Applied Polymer Science*, *139*(24), 52367. doi: 10.1002/app.52367
48. Zhu R., Ji W., Fang B., Wu D., Chen Z., et al. (2017): Ferroelectric phase transition and electrical conduction mechanisms in high Curie-temperature PMN-PHT piezoelectric ceramics. *Ceramics International*, *43*(8), 6417-6424. doi: 10.1016/j.ceramint.2017.02.054
49. Chung T. C., Petchsuk A. (2002): Synthesis and properties of ferroelectric fluoroterpolymers with Curie transition at ambient temperature. *Macromolecules*, *35*(20), 7678-7684. doi: 10.1021/ma020504c
50. Badapanda T., Senthil V., Panigrahi S., Anwar S. (2013): Diffuse phase transition behavior of dysprosium doped barium titanate ceramic. *Journal of Electroceramics*, *31*, 55-60. doi: 10.1007/s10832-013-9808-x
51. Vugmeister B. E., Glinchuk M. D. (1990): Dipole glass and ferroelectricity in random-site electric dipole systems. *Reviews of modern physics*, *62*(4), 993. doi: 10.1103/RevModPhys.62.993
52. Singh S., Kaur A., Kaur P., Singh L. (2023): High-temperature dielectric relaxation and electric conduction mechanisms in a $LaCoO_3$-modified $Na_{0.5}Bi_{0.5}TiO_3$ system. *ACS omega*, *8*(28), 25623-25638. doi: 10.1021/acsomega.3c04490
53. Lu D. Y., Toda M., Sugano M. (2006): High-permittivity double rare-earth-doped barium titanate ceramics with diffuse phase transition. *Journal of the American Ceramic Society*, *89*(10), 3112-3123. doi: 10.1111/j.1551-2916.2006.00893.x
54. Lu D. Y., Ga, X. L., Wang S. (2019): Abnormal Curie-temperature shift in Ho-doped $BaTiO_3$ ceramics with the self-compensation mode. *Results in Physics*, *12*, 585-591. doi: 10.1016/j.rinp.2018.11.094
55. Butee S., Kambale K. R., Ghorpade A., Halikar A., Gaikwad R., Panda H. (2019): Significant improvement in Curie temperature and piezoelectric properties of $BaTiO_3$ with minimum Pb addition. *Journal of Asian Ceramic Societies*, *7*(4), 407-416. doi: 10.1080/21870764.2019.1656359
56. Kuwabara M., Matsuda H., Kurata N., Matsuyama E. (1997): Shift of the Curie point of barium titanate ceramics with sintering temperature. *Journal of the American Ceramic Society*, *80*(10), 2590-2596. doi: 10.1111/j.1151-2916.1997.tb03161.x
57. Gnanasagaran C. L., Ramachandran K., Ramesh S., Ubenthiran S., Jamadon N. H. (2023): Effect of co-doping manganese oxide and titania on sintering behaviour and mechanical properties of alumina. *Ceramics International*, *49*(3), 5110-5118. doi: 10.1016/j.ceramint.2022.10.027

58. Naji I. S., Gatea H. A. (2020): Influence of sintering temperature on ferroelectric $Ba_{0.7}Sr_{0.3}TiO_3$ microstructure, grain size, and electrical properties. *International Journal of Thin Films Science and Technology*, *9*(2), 133-141. doi: 10.18576/ijtfst/090207
59. Gatea H. A., Abbas H., Shaghnab M. L. (2023): Impact of High Heat Treatment on Ferroelectric Materials Properties: $Ba_{1-x}Sr_xTiO_3$ as a Model. *ECS Journal of Solid State Science and Technology*, *12*(8), 083002. doi: 10.1149/2162-8777/acec11
60. Wang X., Huan Y., Zhao P., Liu X., Wei T., Zhang Q., Wang X. (2021): Optimizing the grain size and grain boundary morphology of (K, Na) NbO_3-based ceramics: Paving the way for ultrahigh energy storage capacitors. *Journal of Materiomics*, *7*(4), 780-789. doi: 10.1016/j.jmat.2020.12.009
61. An J. S., Lee H. S., Byeon P., Kim D., Bae H. B., et al. (2023): Unveiling of interstice-occupying dopant segregation at grain boundaries in perovskite oxide dielectrics for a new class of ceramic capacitors. *Energy & Environmental Science*, *16*(5), 1992-2002. doi: 10.1039/D2EE03152C
62. Huan Y., Wei T., Wang X., Liu X., Zhao P., Wang X. (2021): Achieving ultrahigh energy storage efficiency in local-composition gradient-structured ferroelectric ceramics. *Chemical Engineering Journal*, *425*, 129506. doi: 10.1016/j.cej.2021.129506
63. Marincel D. M., Zhang H., Kumar A., Jesse S., Kalinin S. V., Rainforth W. M., et al. (2014): Influence of a single grain boundary on domain wall motion in ferroelectrics. *Advanced Functional Materials*, *24*(10), 1409-1417. doi: 10.1002/adfm.201302457
64. Pramanick A., Prewitt A. D., Forrester J. S., Jones J. L. (2012): Domains, domain walls and defects in perovskite ferroelectric oxides: A review of present understanding and recent contributions. *Critical Reviews in Solid State and Materials Sciences*, *37*(4), 243-275. doi: 10.1080/10408436.2012.686891
65. Buscaglia M. T., Viviani M., Buscaglia V., Mitoseriu L., Testino A., et al. (2006): High dielectric constant and frozen macroscopic polarization in dense nanocrystalline $BaTiO_3$ ceramics. *Physical review B – Condensed matter and materials physics*, *73*(6), 064114.
66. Vikrant K. S. N., Chueh W. C., García R. E. (2018): Charged interfaces: electrochemical and mechanical effects. *Energy & Environmental Science*, *11*(8), 1993-2000. doi: 10.1039/C7EE03400H
67. Greuter F., Blatter G. (1990): Electrical properties of grain boundaries in polycrystalline compound semiconductors. *Semiconductor Science and Technology*, *5*(2), 111. doi: 10.1088/0268-1242/5/2/001
68. Piri A., Aghanajafi C., Sohani A. (2023): Enhancing efficiency of a renewable energy assisted system with adiabatic compressed-air energy storage by application of multiple Kalina recovery cycles. *Journal of Energy Storage*, *61*, 106712. doi: 10.1016/j.est.2023.106712
69. Sun J., Yan G., Fang B., Zhao X., Zhang S., Lu X., Ding J. (2024): Improving energy storage performance of barium titanate-based ceramics by doping MnO_2. *Journal of Energy Storage*, *78*, 110007. doi: 10.1016/j.est.2023.110007
70. Castro R. H. R. (2019): Controlling sintering and grain growth of nanoceramics. *Cerâmica*, *65*(373), 122-129. doi: 10.1590/0366-69132019653732573
71. Eckhardt J. K., Burkhardt S., Zahnow J., Elm M. T., Janek J., Klar P. J., Heiliger C. (2021): Understanding the impact of microstructure on charge transport in polycrystalline materials through impedance modelling. *Journal of The Electrochemical Society*, *168*(9), 090516. doi: 10.1149/1945-7111/ac1cfe
72. Wang S., Frisch S., Zhang H., Yildiz O., Mandal M., Ugur N., et al. (2022): Grain engineering for improved charge carrier transport in two-dimensional lead-free perovskite field-effect transistors. *Materials Horizons*, *9*(10), 2633-2643. doi: 10.1039/D2MH00632D
73. Wang G., Lu Z., Li J., Ji H., Yang H., Li L., et al. (2020): Lead-free (Ba, Sr) TiO_3–$BiFeO_3$ based multilayer ceramic capacitors with high energy density. *Journal of the European Ceramic Society*, *40*(4), 1779-1783. doi: 10.1016/j.jeurceramsoc.2019.12.009
74. Alkathy M., Milton F. P., Zabotto F. L., Gatasheh M. K., Kassim H. A., Raju K. C., & Eiras J. A. (2024): Improve energy storage performance by tweaking grain size and widening the energy bandgap in modified $BaTiO_3$ ceramics. *Indian Journal of Physics*, 1-14. doi: 10.1007/s12648-024-03296-z
75. Alkathy M. S., Milton F. P., Gatasheh M. K., Zabotto F. L., Kassim H. A., Raju K. J., Eiras J. A. (2024): Enhancing dielectric properties and thermal stability in microwave-synthesized Nd-modified barium titanate nanoceramics for possible MLCC applications. *Applied Physics A*, *130*(6), 402. doi: 10.1007/s00339-024-07566-9
76. Alkathy M. S., Gatasheh M. K., Zabotto F. L., Kassim H. A., Raju K. C., Eiras J. A. (2024): Enhancing energy storage performance in $BaTiO_3$ ceramics via Mg and La co-doping strategy. *Journal of Materials Science: Materials in Electronics*, *35*(15), 1-11. doi: 10.1007/s10854-024-12816-w